CHEMISTRY OF MATERIALS
Article

Chem. Mater. **2010,** *22,* 6171–6182 6171
DOI:10.1021/cm1023103

Preparation, Characterization, and Structural Phase Transitions in a New Family of Semiconducting Transition Metal Oxychalcogenides β-$La_2O_2MSe_2$ (M = Mn, Fe)

Emma E. McCabe,[†] David G. Free,[†] Budhika G. Mendis,[‡] Joshua S. Higgins,[‡] and John S. O. Evans*,[†]

[†]*Department of Chemistry and* [‡]*Department of Physics, Durham University, University Science Site, South Road, Durham, DH1 3LE, United Kingdom*

Received August 12, 2010. Revised Manuscript Received October 2, 2010

Two new oxyselenide materials have been synthesized with composition $La_2O_2MSe_2$ (M = Mn, Fe). They adopt a new structure type, the β structure, which has been solved and refined from powder X-ray and neutron diffraction data. The structure is described by *Ama*2 symmetry with unit cell ~17.5 Å × 16.6 Å × 4.0 Å and consists of sheets of MSe_n polyhedra separated by La_2O_2Se blocks. A structural phase transition occurs on cooling involving ordering of M cations and a symmetry reduction to a primitive structure of $Pna2_1$ symmetry. Both manganese and iron analogues are antiferromagnetic at low temperature. β-$La_2O_2FeSe_2$ is a semiconductor in the temperature of 150−300 K with a band gap of approximately 0.7 eV while β-$La_2O_2MnSe_2$ is insulating at room temperature with band gap of 1.6 eV.

Introduction

While research into the structural chemistry and physical properties of complex metal oxide systems has been extremely fruitful, the importance of mixed anion systems, containing an oxide as well as another anion type involved in metal bonding, has been highlighted recently by the discovery of superconductivity in the iron oxyarsenide systems.[1] Oxychalcogenide materials contain oxide anions and a heavier group 16 anion and, owing to the different chemical nature of these anions, frequently adopt layered structures allowing segregation of the two anions; a review of these materials has been published by Clarke et al.[2] One well-known family of oxychalcogenides are *Ln*CuOS (*Ln* = La-Nd) materials, which are wide-gap p-type semiconductors which exhibit photoluminescent properties.[3] These adopt the ZrCuSiAs structure and are built up of alternating layers of fluorite-like edge-shared OLa_4 tetrahedra and layers of antifluorite-like edge-shared CuS_4 tetrahedra.[4] The superconducting iron oxyarsenides *Ln*FeOAs also adopt this structure type with the fluorite-like $[Ln_2O_2]^{2+}$ layers acting as charge reservoirs which can be doped to induce superconductivity in the $[Fe_2As_2]^{2-}$ layers.[1]

The majority of oxyselenides in the ZrCuSiAs family contain layers of edge-shared $Cu(S,Se)_4$ tetrahedra containing formally Cu^+ cations, although two analogues containing divalent metal cations have been reported: in $CeMn_{0.5}OSe$, the tetrahedral sites in the antifluorite layers are half-occupied by Mn^{2+} in a disordered fashion[5] while in $La_2O_2CdSe_2$, the vacancies are ordered giving rise to $[CdSe_2]^{2-}$ layers containing corner-linked $CdSe_4$ tetrahedra.[6] As part of our work into the synthesis and properties of transition metal-containing oxychalcogenides, we have prepared several new layered materials related to $CeMn_{0.5}OSe$ (to be reported elsewhere). We have also synthesized a family of materials which adopt a new structure type, which we label β to distinguish them from the layered structures, with formula $La_2O_2MSe_2$ (M = Mn, Fe); we report here the synthesis of β-$La_2O_2MSe_2$ (M = Mn, Fe) and their structure solution from powder diffraction data as well as a detailed investigation of their structure and phase transitions as a function of temperature using X-ray and neutron powder diffraction data. We also report physical properties of β-$La_2O_2MSe_2$ from conductivity and magnetic measurements and diffuse reflectance spectroscopy.

Experimental Section

Polycrystalline samples of β-$La_2O_2MnSe_2$ and β-$La_2O_2FeSe_2$ were prepared by the reaction of La_2O_3 (99.9%, Sigma-Aldrich,

*To whom correspondence should be addressed. Email: john.evans@durham.ac.uk.

(1) Kamihara, Y.; Watanabe, T.; Hirano, M.; Hosono, H. *J. Am. Chem. Soc.* **2008**, *130*, 3296–3297.
(2) Clarke, S. J.; Adamson, P.; Herkelrath, S. J. C.; Rutt, O. J.; Parker, D. R.; Pitcher, M. J.; Smura, C. F. *Inorg. Chem.* **2008**, *47*, 8473–8486.
(3) Ueda, K.; Takafuji, K.; Hiramatsu, H.; Ohta, H.; Kamiya, T.; Hirano, M.; Hosono, H. *Chem. Mater.* **2003**, *15*, 3692–3695.
(4) Johnson, V.; Jeitschko, W. *J. Solid State Chem.* **1974**, *11*, 161–166.
(5) Ijjaali, I.; Mitchell, K.; Haynes, C. L.; McFarland, A. D.; Duyne, R. P. V.; Ibers, J. A. *J. Solid State Chem.* **2003**, *176*, 170–174.
(6) (a) Hiramatsu, H.; Ueda, K.; Kamiya, T.; Ohta, H.; Hirano, M.; Hosono, H. *J. Mater. Chem.* **2004**, *14*, 2946–2950. (b) Hiramatsu, H.; Ueda, K.; Kamiya, T.; Ohta, H.; Hirano, M.; Hosono, H. *J. Phys. Chem. B* **2004**, *108*, 17344–17351.

Published on Web 10/29/2010

heated to 1000 °C prior to use), Se (99.999%, Alfa-Aesar), and Mn (99%+, Avocado) or Fe (99.9%, Sigma-Aldrich) powders in a molar ratio 1:2:1. These reagents were intimately ground together using an agate pestle and mortar and placed in an alumina crucible. Al powder (10% molar excess) was placed in a second alumina crucible to act as an oxygen getter (forming Al_2O_3 during the reaction). These two crucibles were placed inside a quartz tube which was evacuated, sealed, and then heated slowly to 1100 °C and held at this reaction temperature for 12 h. β-$La_2O_2MnSe_2$ was furnace-cooled to room temperature while β-$La_2O_2FeSe_2$ was quenched from 1100 °C into iced water (unquenched samples of β-$La_2O_2FeSe_2$ contained a significant amount of iron metal). β-$La_2O_2MnSe_2$ thus prepared is a brick-red powder whereas β-$La_2O_2FeSe_2$ is black. The β-$La_2O_2MnSe_2$ sample contained a ~2% impurity phase which has not been identified. Aliovalent doping with Ca^{2+} substituted for La^{3+} has not been successful to date. Substituting O^{2-} by F^- in β-$La_2O_2FeSe_2$ gave a small change in unit cell parameters, suggesting solid solution but no significant change in physical properties.

X-ray powder diffraction (XRPD) data were collected on a Bruker D8 diffractometer (reflection mode, Cu $K\alpha_1/K\alpha_2$ radiation, Lynxeye Si strip position sensitive detector, step size 0.02° with variable slits) equipped with an Oxford Cryosystems PheniX cryostat or an Anton Paar HTK1200 furnace. Samples were sprinkled onto a zero-background Si wafer (or an amorphous SiO_2 disk for use in the furnace) and held in place with a thin layer of Vaseline. Data were collected over a period of 12 h at 300 and 12 K in the 2θ range of 5−120° for both samples. Twenty minute scans were also collected at 5 K intervals on cooling and warming between 12 and 300 K. Room temperature time-of-flight (TOF) neutron powder diffraction (NPD) data were collected on ~1 g of β-$La_2O_2MnSe_2$ on the GEM diffractometer at the ISIS facility of the Rutherford Appleton Laboratory (via the GEM Xpress scheme). TOF NPD data were also collected for both samples using the HRPD diffractometer, also at the ISIS facility. Approximately 2 g of material were mounted in vanadium slab cans. Data were collected from 12 to 366 K in 6 K steps over the TOF range of 10−210 ms (2.5 μA h scans at each temperature) for β-$La_2O_2MnSe_2$, and over the TOF range of 30−230 ms for β-$La_2O_2FeSe_2$ (collecting 7.5 μA h scans below 156 K and 2.5 μA h scans from 162 to 366 K). In addition, long scans (66 μA h) were also collected at 12 and 295 K for both samples. Powder diffraction data were analyzed by the Rietveld method using the TOPAS Academic (TA) software suite controlled by local routines.[7] Short scans were analyzed to determine the temperature dependence of lattice parameters, and combined structural refinements were performed using long scans. The background (shifted Chebyshev) zero point or sample height, (DIFA/DIFC for neutron refinements), peak profiles (pseudo-Voigt), lattice parameters, atomic positions, site occupancies, atomic displacement parameters, and minor impurity content were typically refined. Some scattering from vanadium was observed in the NPD data, presumably from the sample can. A vanadium phase was, therefore, included in neutron refinements. Estimates of magnetic ordering temperatures were made from the short neutron scans using a parametric fitting approach.[8] The low q range of all powder patterns were fitted simultaneously with a smoothed, temperature-dependent background function. The intensities of magnetic only reflections were controlled by an expression of the form $(1 - T/T_N)^\beta$ with T_N and β allowed to refine.

Selected area electron diffraction (SAED) data were collected using a Joel 2100F transmission electron microscope operating at 200 keV. The sample was deposited onto a holey carbon grid. This was mounted in a double-tilt sample holder, and zone-axis diffraction patterns were acquired using a Gatan Orius CCD camera.

Magnetic measurements were carried out using a Quantum Design SQUID magnetometer with an applied magnetic field of 1000 Oe in the temperature range of 2−292 K. Four-probe measurements for conductivity data were carried out using a Quantum Design Physical Properties Measurement System (PPMS) with copper electrodes attached with silver paste. The samples were tested for second-harmonic generation (SHG) using the experimental setup described in ref 9.

The diffuse reflectance spectra were recorded by placing a sample ground with dry sodium chloride (~1% w/w) in an optical cuvette and illuminating it with the focused output of a tungsten lamp (Ocean Optics HL-2000). Nonspecular scattered light was collected, and the spectrum was recorded using a CCD-spectrograph combination (Avantes Avaspec 2048-FT). A cuvette of ground sodium chloride was used as a reference. The data were used to calculate the reflectance spectra R(I) and Kubelka−Munk spectra F(R).[10]

Results and Discussion

Structure Solution and Refinement. The unit cell of β-$La_2O_2MnSe_2$ was initially indexed from a 20 min XRPD pattern using the indexing routines in TA.[7] This successfully indexed all the observed reflections using a 17.5 × 16.6 × 4.0 Å unit cell, giving a unit cell with volume approximately eight times that expected for a ZrCuSiAs-type material of composition $LaMn_{0.5}OSe$. To solve the structure, high quality XRPD data were collected over a 2θ range of 5−120° for 15 h; indexing of these data were consistent with the initial results. ExtSym[11] was also used to investigate the symmetry and suggested extinction symbols *A--c* and *A*2_1--; however, Pawley refinements[12] showed that *A*$2_1$22 (nonstandard setting of *C*222$_1$) gave a much better fit to the observed data. Structure solution was performed using two techniques: charge flipping and direct methods. Charge flipping[13] was performed in TA with cell contents eight times that of ZrCuSiAs-type $LaMn_{0.5}OSe$. This method was successful in identifying the La^{3+} and Mn^{2+}/Se^{2-} positions. This trial structure was confirmed using direct methods in EXPO.[14]

(7) (a) Coelho, A. A. *J. Appl. Crystallogr.* **2003**, *36*, 86.(b) Coelho, A. A. *TOPAS Academic: General Profile and Structure Analysis Software for Powder Diffraction Data*, edition 4.1; Bruker AXS: Karlsruhe, Germany, 2007.
(8) (a) Stinton, G. W.; Evans, J. S. O. *J. Appl. Crystallogr.* **2007**, *40*, 87–95. (b) Evans, J. S. O. *Mater. Sci. Forum* **2010**, *65*, 1–9.
(9) Ok, K. M.; Chi, E. O.; Halasyamani, P. S. *Chem. Soc. Rev.* **2006**, *35*, 710–717.
(10) Kortum, G.; Braun, W.; Herzog, G. *Angew. Chem., Int. Ed.* **1963**, *2* (7), 333–404.
(11) Markvarsden, A. J.; Shankland, K.; David, W. I. F.; Johnston, J.; Ibberson, R. M.; Tucker, M.; Nowell, H.; Griffin, T. *J. Appl. Crystallogr.* **2008**, *41*, 1177.
(12) Pawley, G. S. *J. Appl. Crystallogr.* **1981**, *14*, 357.
(13) Oszlanyi, G.; Suto, A. *Acta Crystallogr.* **2008**, *A64*, 123.
(14) (a) Altomare, A.; Burla, M. C.; Cascarano, G.; Giacovazzo, C.; Guagliardi, A.; Moliterni, A. G. G.; Polidori, G. *J. Appl. Crystallogr.* **1995**, *28*, 842. (b) Altomare, A.; Cascarano, G.; Giacovazzo, C.; Guagliardi, A.; Burla, M. C.; Polidori, G.; Camalli, M. *J. Appl. Crystallogr.* **1994**, *27*, 435.

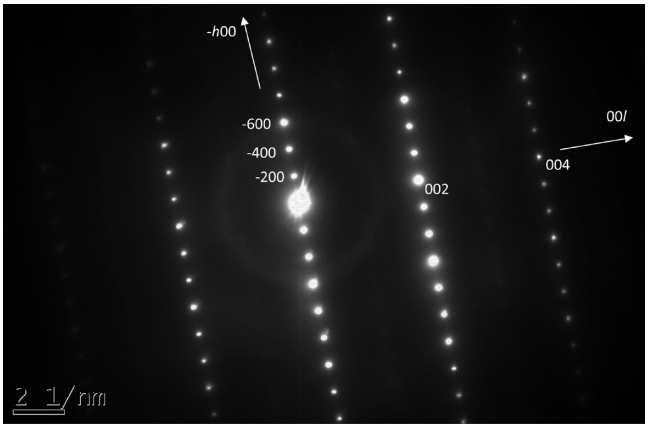

Figure 1. SAED patterns taken down the [010] zone axis at room temperature for β-$La_2O_2MnSe_2$.

The partial structural model was developed using full Rietveld analysis.[15] From a combination of fractional occupancy refinements of proposed sites and comparison with chemically similar systems, a model giving excellent agreement to observed data was obtained. Examination of the structure suggested the possibility of higher symmetry and refinement in *Amam* ($\bar{c}$ba setting of *Cmcm*; $A2_122$ is a maximal subgroup of *Amam*) gave good fits to the both the XRPD and NPD data (for *Amam*, R_{wp} = 4.359% with 81 independent parameters, and for $A2_122$, R_{wp} = 4.344% with 84 independent parameters) and a structural model very similar to that in $A2_122$. Reflection conditions for $A2_122$ and *Amam* are very similar, differing only for *h0l* reflections; for $A2_122$, reflections with $l = 2n$ are allowed, while *Amam* has the additional condition that h, $l = 2n$. Pawley fits were used to determine the intensity of the *h0l* $h \neq 2n$ reflections; no significant intensity was observed (giving no evidence for the loss of the *a* glide), so space group $A2_122$ (and similarly *Amm*2 symmetry) was not considered further. This conclusion is supported by room temperature electron diffraction data shown in Figure 1. Diffraction patterns taken down the [010] zone axis show *h0l* reflections for which $h, l = 2n$ and no intensity was observed for $h \neq 2n$ reflections.

While a model of *Amam* symmetry describes the diffraction data well and gave a sensible structural model, β-$La_2O_2MnSe_2$ was found to be weakly second harmonic generation (SHG) active at room temperature, suggesting that an acentric model of polar, piezoelectric point-group *mm*2 would be more appropriate to describe the structure than one of point-group *mmm*.[9,16] Two possible space groups are then possible: loss of the mirror plane perpendicular to *a* in *Amam* gives space group $A2_1am$ but results in one-half-occupied Mn(2) site (8*f* in *Amam*) becoming two distinct 4*a* sites in $A2_1am$ which seemed unlikely given the low temperature behavior described below; loss of the mirror plane perpendicular to *c* in *Amam* to give *Ama*2 symmetry maintains the multiplicity of the occupied atom sites. A refinement was, therefore, performed in *Ama*2 symmetry and gave a good fit to the data (R_{wp} = 4.307%, 98 independent parameters). The structural model is shown in Figure 2. Refinement profiles are shown in Figure 3; details of the refinement are given in Table 1, and bond lengths are in Table 2. Bond valence sum calculations gave +2.04 and +1.91 for Mn(1) and Mn(2) cations and +2.96 and +3.06 for La(1) and La(2), respectively.[17]

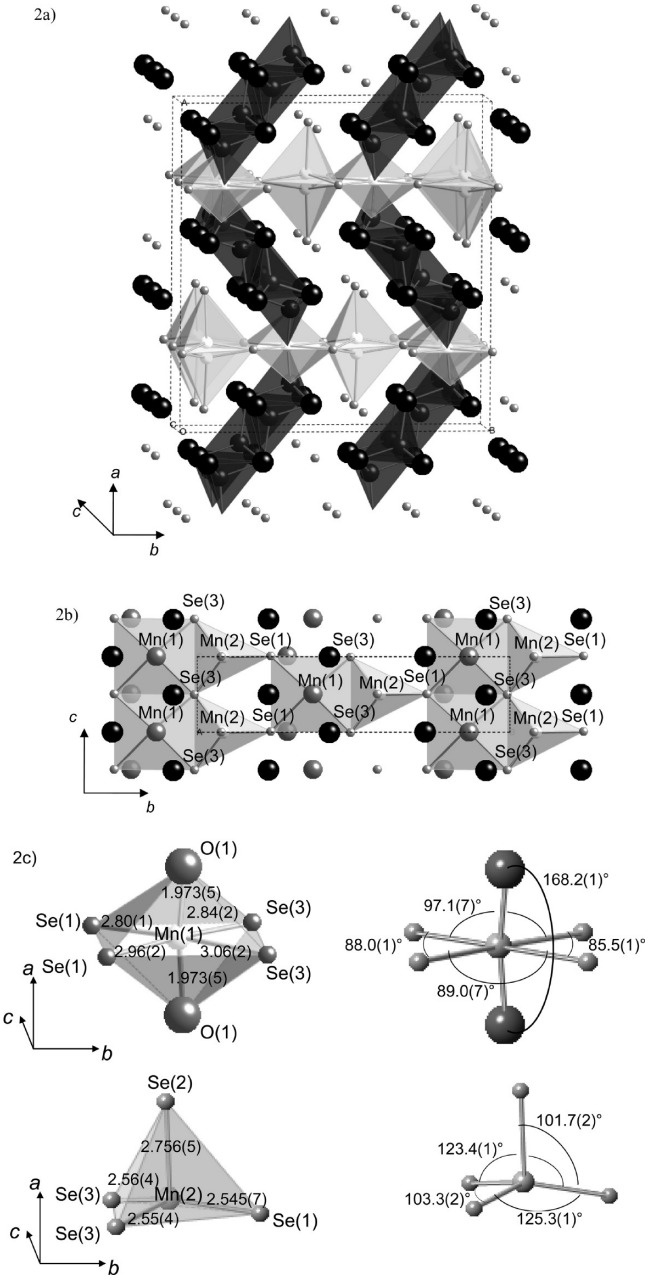

Figure 2. Room temperature structure of β-$La_2O_2MnSe_2$ described in *Ama*2 viewed down [001] direction (a) and down [100] direction showing connectivity of MnSe plane (b), with MnSe polyhedra in light gray and OLa_4 tetrahedra in dark gray with Se and La atoms shown as gray and black spheres, respectively, and (c) showing bond lengths (in Å) and angles of Mn(1) and Mn(2) polyhedra.

The structure of β-$La_2O_2MnSe_2$ can be described in several different ways. One viewpoint is to consider it in terms of MnSe layers perpendicular to [100]. These MnSe

(15) Rietveld, H. M. *J. Appl. Crystallogr.* **1969**, *2*, 65.
(16) Halasyamani, P. S.; Poeppelmeier, K. R. *Chem. Mater.* **1998**, *10*, 2753–2769.
(17) (a) Brown, I. D.; Altermatt, D. *Acta Crystallogr.* **1985**, *B41*, 244–247. (b) Brese, N. E.; O'Keefe, M. *Acta Crystallogr.* **1991**, *B47*, 192–197.

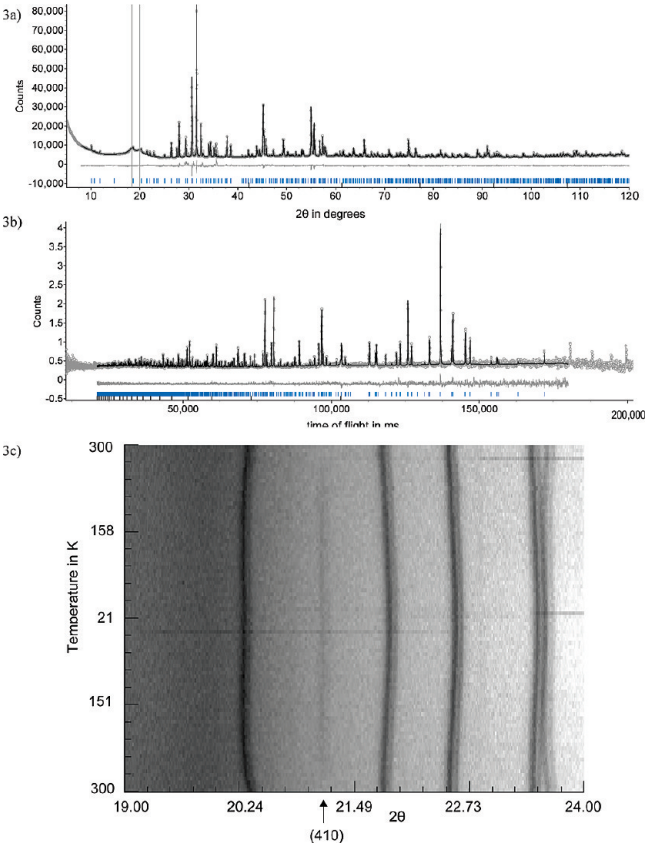

Figure 3. Rietveld refinement profiles from combined refinement using room temperature XRPD (a) and NPD backscattered data (b) for β-$La_2O_2MnSe_2$, refined in space group *Ama*2 (observed and calculated patterns shown in gray and black, respectively, with difference profile and peak positions shown below in gray given by vertical tick marks) and (c) film plot of 19−24° 2θ region as a function of temperature showing appearance of (410) reflection.

Table 1. Structural Parameters from Combined Refinement for β-$La_2O_2MnSe_2$ Using Room Temperature XRPD and NPD (Backscattered) Data[a]

	Wyckoff site	*x*	*Y*	*z*	occupancy	B_{eq}/Å^2
Mn(1)	4*b*	0.25	0.8612(3)	0.035(4)	1	0.5(1)
Mn(2)	8*c*	0.2264(3)	0.0842(4)	0.00(1)	0.5	0.5(1)
La(1)	8*c*	0.40955(9)	0.72984(9)	0[b]	1	0.45(5)
La(2)	8*c*	0.41526(8)	0.9246(1)	0.490(2)	1	0.29(5)
O(1)	8*c*	0.3620(2)	0.3707(3)	0.503(8)	1	0.24(8)
O(2)	8*c*	0.0445(3)	0.2906(2)	0.006(7)	1	0.07(8)
Se(1)	4*b*	0.25	0.2359(2)	0.006(5)	1	0.47(8)
Se(2)	8*c*	0.4307(1)	0.0775(1)	0.002(4)	1	0.83(6)
Se(3)	4*b*	0.25	0.4918(1)	−0.003(6)	1	0.42(7)

[a] Space group *Ama*2, a = 17.52751(7) Å, b = 16.54578(8) Å, c = 4.00738(2) Å; R_{wp} = 4.307%, R_p = 2.862%, and χ^2 = 4.94. [b] Coordinate fixed as origin not defined along z in space group *Ama*2.

sheets contain chains of edge-shared $Mn(1)Se_4O_2$ octahedral chains with $Mn(2)Se_n$ polyhedra edge and corner linked to the chains. The Mn(2) site is found to be 50:50 disordered over two sites on either side of the central MnSe planes. The Mn(2) coordination environment can, therefore, be described as trigonal bipyramidal if Mn(2) occupied the average position or, more realistically, as a series of disordered $Mn(2)Se_4$ tetrahedra above and below the MnSe planes. The disordered Mn(2) site (8*c*) is displaced from the ideal 4*b* site in the MnSe plane by a distance of 0.83 Å, and bond angles are shown in Figure 2c. The trans $MnSe_4O_2$ octahedra are similar to the $FeSe_4O_2$ octahedra found in $La_2O_2Fe_2OSe_2$.[18] We have, therefore, a 1:1 mix of the transition metal coordination environment found in this and the LnFeOAs related systems. The MnSe sheets are separated by La_2O_2Se ribbons four Ln_4O tetrahedra wide separated by Se anions which are arranged in a herringbone fashion, bridging the MnSe layers. An alternate view is to describe the structure in terms of anion segregation. In this viewpoint, one has corrugated layers of Se^{2-} anions perpendicular to [010] which coordinate to a mixture of Mn and La cations. Oxide ions are exclusively found in four-coordinate M_4O tetrahedral environments with 50% of oxide ions in an La_4O environment and 50% in an La_3MnO environment. La ions are in eight-coordinate sites coordinated to four oxide and four selenide anions. *Ama*2 is a polar space group, with c as the polar axis, and structural refinements suggest that Mn(1) is slightly displaced from the center of its polyhedron along the [001] direction (~0.13 Å at room temperature).

This structure type has not been previously reported to the best of our knowledge but contains features common to other quaternary oxychalcogenides. For example, the edge-shared OLa_4 tetrahedra are a four tetrahedra-wide portion of the infinite sheets found in the ZrCuSiAs materials such as LaCuOSe[19] and the oxypnictides

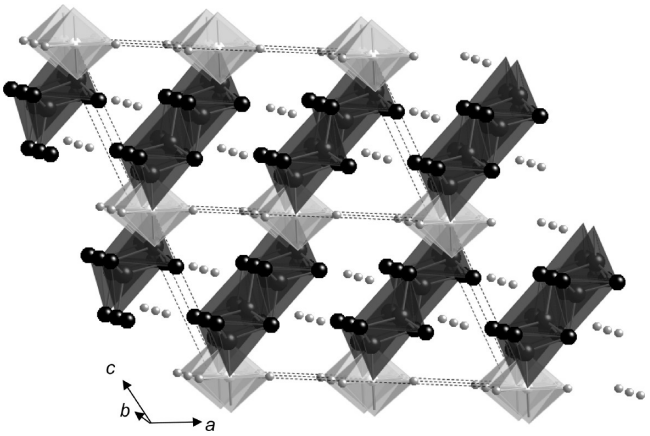

Figure 4. Illustration of the $Gd_4O_4TiSe_4$ crystal structure (*C*2/*m* symmetry), showing TiSe polyhedra in light gray and OGd_4 tetrahedra in dark gray with Se and Gd atoms shown as gray and black spheres, respectively.

Table 2. Selected Bond Lengths for β-$La_2O_2MnSe_2$ from Combined Refinement Using Room Temperature XRPD and NPD (Backscattered) Data in Space Group *Ama*2

Mn(1)−O(1)	2 × 1.973(5) Å	La(1)−O(1)	2.475(5) Å
Mn(1)−Se(1)	2.80(1) Å, 2.96(2) Å	La(1)−O(2)	2.36(2) Å, 2.390(5) Å, 2.40(2) Å
Mn(1)−Se(3)	2.84(2) Å, 3.06(2) Å	La(2)−O(1)	2.43(2) Å, 2.34(2) Å
Mn(2)−Se(1)	2.545(7) Å	La(2)−O(2)	2.328(5) Å
Mn(2)−Se(2)	2.756(5) Å	La(2)−Se(3)	3.103(2) Å
Mn(2)−Se(3)	2.55(4) Å, 2.56(4) Å		

(18) Mayer, J. M.; Schneemeyer, L. F.; Siegrist, T.; Waszczak, J. V.; Dover, B. V. *Angew. Chem.* **1992**, *104*(12), 1677–1678.
(19) Hiramatsu, H.; Yanagi, H.; Kamiya, T.; Ueda, K.; Hirano, M.; Hosono, H. *Chem. Mater.* **2008**, *20*, 326–334.

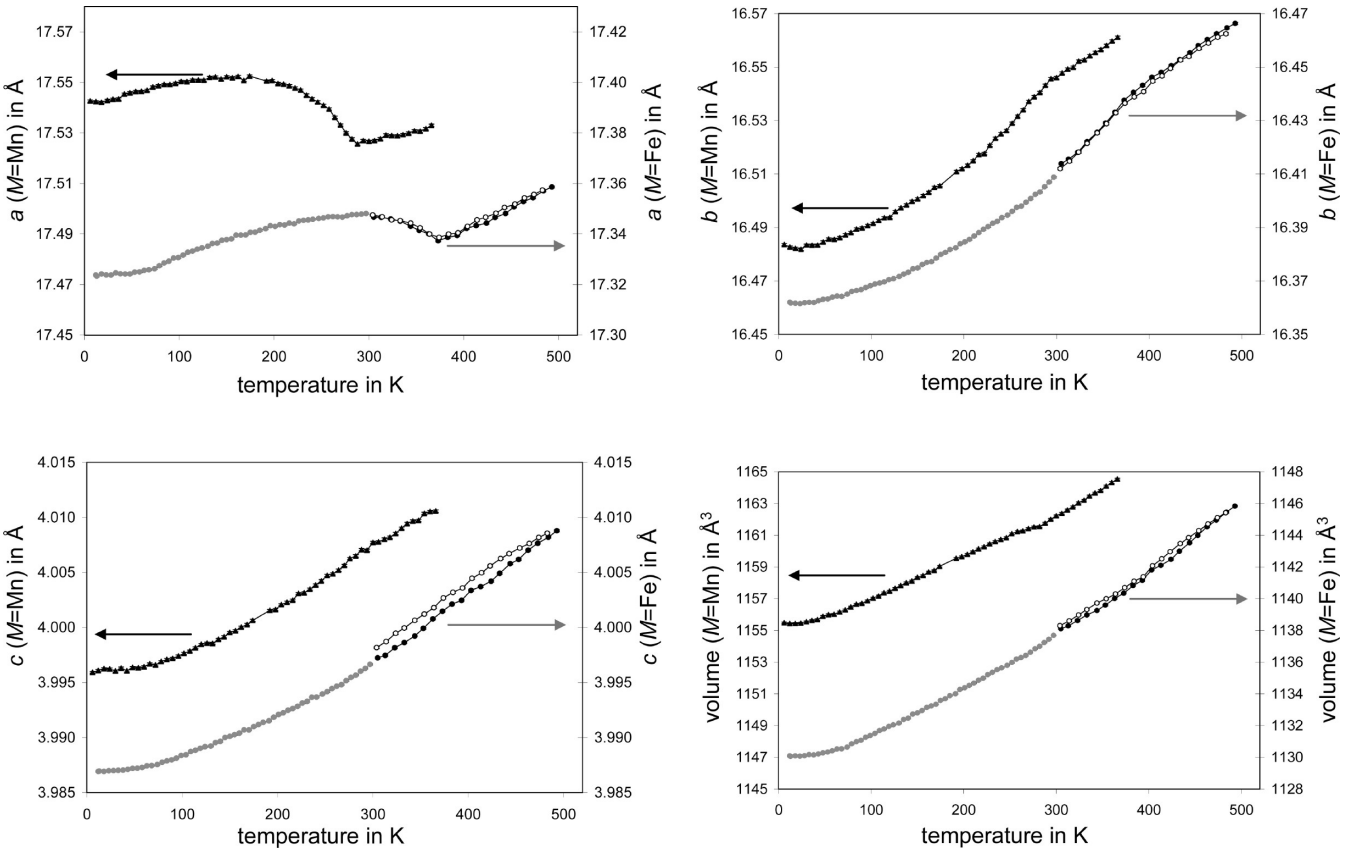

Figure 5. Lattice parameters of β-$La_2O_2MSe_2$ as a function of temperature, obtained from refinement using NPD data shown for M = Mn (shown by black triangles) and XRPD data for M = Fe (gray circles low temperature XRPD data, warming/cooling high temperature XRPD data shown with closed and open circles, respectively).

LaFeOAs.[1] An interesting structure containing these units is $La_4O_4Ti_2Se_5$, made up of edge-sharing OLa_4 tetrahedra arranged in broken-fluorite sheets, and TiO_2Se_4 octahedra extending along the [100] direction and undulating in the *bc* plane.[20] The structure that is most closely related to $La_2O_2MnSe_2$ is perhaps that reported for $Gd_4O_4TiSe_4$ (illustrated in Figure 4).[21] $Gd_4O_4TiSe_4$ ($Gd_2O_2SeTi_{0.5}Se$) is composed of gadolinium oxide blocks at ~62° to the TiSe layers, comparable with the lanthanum oxide blocks at ~64° to the MnSe layers in β-$La_2O_2MnSe_2$. However, while these gadolinium oxide blocks on either side of the TiSe layers are parallel in $Gd_4O_4TiSe_4$, those in β-$La_2O_2MnSe_2$ are related by screw axes along *c* and so are at an angle of ~128° to one another. The distance between TiSe layers in $Gd_4O_4TiSe_4$ and between MSe layers in β-$La_2O_2MnSe_2$ are comparable, approximately 8.56 Å for $Gd_4O_4TiSe_4$ and 8.76 Å for β-$La_2O_2MnSe_2$. It is useful to compare the cation sites in the two structures: small Ti^{4+} cations occupy the octahedrally coordinated sites at either end of the Gd_2O_2 blocks in $Gd_4O_4TiSe_4$, equivalent to the Mn(1) sites in β-$La_2O_2MnSe_2$. However, the Mn(2) site of β-$La_2O_2MnSe_2$ is vacant in $Gd_4O_4TiSe_4$ as an additional cation is not required for charge balance.

Low Temperature Phase Transition in β-$La_2O_2MnSe_2$. On cooling β-$La_2O_2MnSe_2$, an additional very weak reflection was observed in XRPD patterns at ~21° 2θ which could not be matched to likely impurity phases but could be indexed as the 410 reflection of the cell described above. Slower XRPD scans were then collected over a narrow 2θ window (19−24° 2θ) in order to investigate the appearance of this very weak reflection (see film plot shown in Figure 3c). Although weak, the 410 reflection appears on cooling below ~255 K and disappears on warming above ~255 K and showed no hysteresis on the time scale of the diffraction experiments (~15 K h^{-1}). This reflection disobeys the reflection condition $k + l = 2n$ and so is inconsistent with *A*-centering. No significant additional short *d*-spacing reflections were observed in the low temperature NPD data.

The unit cell parameters of β-$La_2O_2MnSe_2$ were determined from XRPD and NPD data between 12 and 366 K. Those derived from the HRPD back scattering bank are shown in Figure 5a. While the *b* and *c* unit cell parameters increased smoothly with increasing temperature, there was a slight change in gradient in cell volume and a significant deviation in *a* unit cell parameter at ~260 K. On warming β-$La_2O_2MnSe_2$ from 6 to 366 K, *a* decreased by 0.06%, while *b*, *c*, and the cell volume increased by 0.47%, 0.37%, and 0.78%, respectively.

These results suggest that β-$La_2O_2MnSe_2$ undergoes a continuous structural phase transition at ~255 K which is fully reversible. From our knowledge of the room temperature structure, it seemed likely that this phase

(20) Tougait, O.; Ibers, J. A. *J. Solid State Chem.* **2001**, *157*, 289–295.
(21) Meerschaut, A.; Lafond, A.; Meignen, V.; Deudon, C. *J. Solid State Chem.* **2001**, *162*, 182–187.

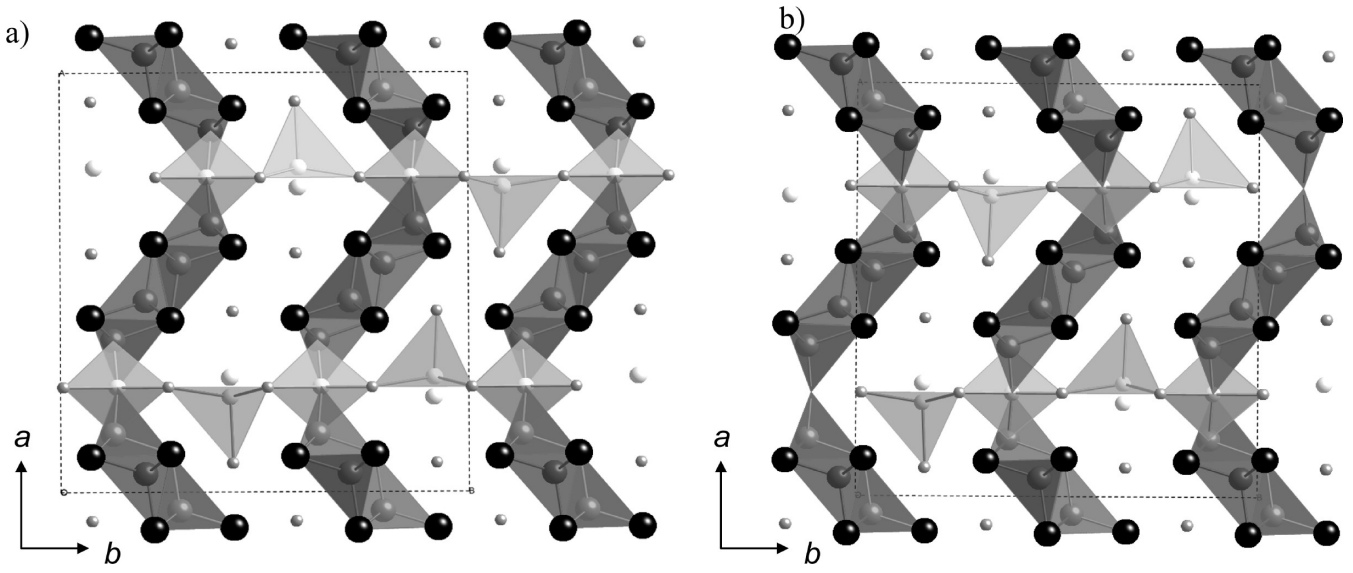

Figure 6. Illustration of possible ordered structures for β-$La_2O_2MnSe_2$ below 260 K resulting from (a) Y2 ordering to give a structure of *Pnn*2 symmetry and (b) Y3 ordering to give a structure of $Pna2_1$ symmetry.

transition, involving loss of *A*-centering to give a low temperature structure of primitive symmetry, could be related to ordering of the Mn(2) sites.

Using a symmetry-adapted distortion mode refinement methodology, the possible low temperature ordered structures can be described in terms of the parent *Ama*2 structure and a number of possible ordering modes. These occupancy modes were explored using the web-based ISODISPLACE[22] package. For example, the occupancy mode with the full ISODISPLACE label *Ama*2[0,0,0] Γ1(a)[Mn2:c]order(a), which we refer to here as Γ1, gives rise to an overall increase or decrease in occupancy of all Mn(2) sites and, hence, no change in symmetry. Occupancy modes associated with other irreducible representations do give rise to changes in symmetry and hence describe a transition to a subgroup of the parent structure. The occupancy modes Γ2, Γ3, Y2, and Y3 all allow the occupancy of Mn(2) sites within a pair (pairs of 8c sites in the *Ama*2 model) to be inversely related and so can give rise to chemically sensible ordered structures. Γ2 and Γ3 modes allow the occupied sites within a given MnSe sheet to be either all above or all below the sheet (i.e., no alternation from one side of the sheet to the other along the [010] direction). The ordering pattern is the same from sheet to sheet for Γ3 and alternates from one side of the sheet to the other along the [100] direction for Γ2. The occupancy modes Y2 and Y3 allow the occupied sites within an MnSe sheet to alternate from one side of the sheet to the other along the [010] direction. With Y2 ordering, this pattern alternates from sheet to sheet along the [100] direction, so that both Mn(2) sites between adjacent La_2O_2 blocks are either occupied or vacant (see Figure 6a). For Y3 ordering, the pattern does not alternate along the [100] direction and so, of the two possible Mn(2) sites between adjacent La_2O_2 blocks, one would be occupied and one would be vacant (see Figure 6b).

(22) Campbell, B. J.; Stokes, H. T.; Tanner, D. E.; Hatch, D. M. *J. Appl. Crystallogr.* **2006**, *39*, 607–614.

Table 3. Summary of Maximal Subgroups of *Ama*2 and Possible Mn(2) Cation Arrangements

space group	occupancy modes	Mn(2) arrangement	410 reflection
*Ama*2	Γ1	disordered	forbidden
*A*112 (*C*2)	Γ2	ordered	forbidden
*A*1*a*1 (*Cc*)	Γ3	ordered	forbidden
*Am*11 (*Pm*)	Γ4	disordered	forbidden
*Pma*2	Y1	disordered	allowed
*Pnn*2	Y2	ordered	allowed
$Pna2_1$	Y3	ordered	allowed
$Pmn2_1$	Y4	disordered	allowed

Since the transition was continuous in nature, space groups that are maximal subgroups of *Ama*2 were considered to describe the low temperature polymorph, and our distortion mode analysis allows us to identify an appropriate symmetry description of the low temperature structure. The seven maximal subgroups are listed in Table 3 and symmetry-allowed occupancy modes are also listed. Although *A*112 and *A*1*a*1 symmetries both allow Mn(2) ordering (due to nonzero amplitude of either Γ2 or Γ3 occupancy modes), the *A*-centering is retained in the ordered structure and so ordering would not give rise to any intensity in the 410 reflection. In addition, no peak broadening or splitting was observed on cooling, making a transition to a monoclinic structure unlikely. *Pnn*2 and $Pna2_1$ models allow Mn(2) ordering and result in loss of *A*-centering and so are consistent with observation of the 410 reflection.

To confirm the identity of the ordering mode and, hence, the symmetry of the low temperature structure, a refinement was carried out using XRPD data collected at 12 K over a period of 12 h. A structural model of *Ama*2 symmetry was used, and the amplitude of all eight possible occupancy modes were refined in turn (applying all eight occupancy modes gives a hypothetical model of *P*1 symmetry and is equivalent to refining all site occupancies independently). The R_{wp} for refinements with different occupancy modes are shown in Figure 7. Refining the amplitude of the Y3 mode gave the largest reduction in

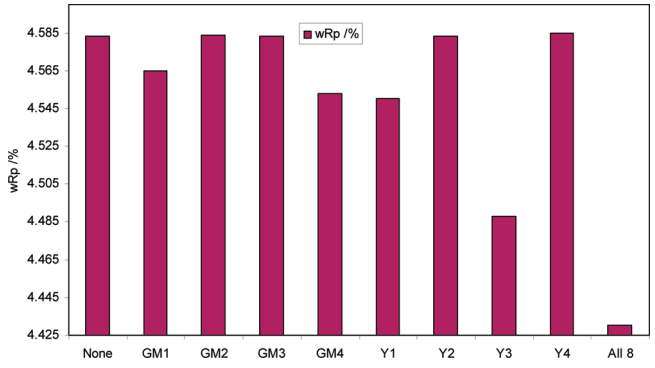

Figure 7. Decrease in R_{wp} as different occupancy modes were refined to fit XRPD data collected at 12 K for β-$La_2O_2MnSe_2$.

R_{wp} and it is clear that Y3 describes the ordering in β-$La_2O_2MnSe_2$ better than any other mode, suggesting the low temperature space group is $Pna2_1$. The Y3/$Pna2_1$ model also leads to favorable local bonding: on ordering, the "apical" Se anion is likely to move closer to the occupied 4*a* site to optimize Mn(2) bonding; in a model of *Pnn*2 symmetry, this might leave the La cations underbonded with both Se anions between adjacent La_2O_2 blocks involved in bonding to occupied 4*a* Mn(2) sites; in a model of $Pna2_1$ symmetry, only one Se anion between adjacent La_2O_2 blocks will be involved in bonding to an occupied 4*a* site, leaving the other Se anion to move away from the vacant 4*a* site and closer to the La cations, fulfilling their bonding requirements.

Using the TA software and Multitopas,[23] the amplitudes of the distortion modes that become active on going from *Ama*2 to $Pna2_1$ were refined as a function of temperature against XRPD data collected over the 2θ range of 8−120°. The irreducible representation Y3 contains several displacement modes and an occupancy mode that refined to nonzero amplitudes with decreasing temperature. The most significant of these distortion modes was the Y3−Mn(2) occupancy mode which describes ordering of the Mn(2) cations over the 4*a* sites above and below the MnSe plane. The dependence of the Y3−Mn(2) occupancy mode amplitude with temperature is shown in Figure 8. Although the quality of the data is low, the mode amplitude has been fitted to a $(1 - T/T_c)^{\beta}$ temperature dependence with values of T_c and β of 272(1) K and 0.22(4), respectively. While the intensity difference between calculated patterns for the low temperature and high temperature phases is extremely small, the clear temperature dependence of occupancy mode (and hence Mn(2) site ordering) observed from these sequential refinements provides good evidence that this structural phase transition relates to Mn(2) ordering.

Conventional combined refinements using XRPD data and NPD data collected at 12 K were then carried out for β-$La_2O_2MnSe_2$. Allowing the Mn(2) occupancy over the 4*a* sites to refine improved the refinement (R_{wp} dropped

(23) (a) Evans, J. S. O. *Multitopas-Fortran 77 routine*. Durham University, Durham, United Kingdom, 1999. (b) Campbell, B. J.; Evans, J. S. O.; Perselli, F.; Stokes, H. T. *IUCr Newsletter* **2007**, *8*(November), 81–95.

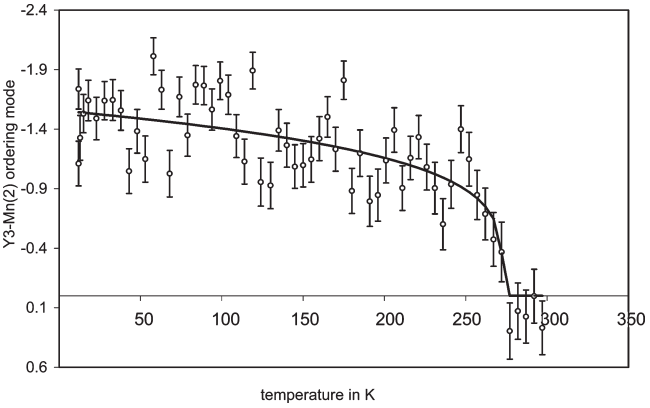

Figure 8. Amplitude of occupancy modes Y3−Mn(2) as a function of temperature with observed points shown as closed circles and calculated values for a function with T_C refined as 273 K shown with open circles from distortion mode refinements using XRPD data for $La_2O_2MnSe_2$. The occupancy of the Mn(2) sites, Mn2_a and Mn2_b is given by occ(Mn2_a) = 0.5 + (0.35355 × b3); occ(Mn2_b) = 0.5 − (0.35355 × b3) where b3 is the amplitude of the Y3−Mn(2) occupancy mode.

Table 4. Structural Parameters from Combined Refinement for β-$La_2O_2MnSe_2$ Using 12 K XRPD and NPD (Backscattered) Data[a]

	Wyckoff site	*x*	*y*	*z*	occupancy	B_{eq}/Å^2
Mn(1)	4*a*	0.2572(5)	0.8882(2)	−0.035(4)	1	−0.4(1)
Mn(2)	4*a*	0.7766(2)	0.3353(3)	0.478(4)	1	−0.4(1)
La(1)	4*a*	0.5910(2)	0.4769(2)	0[b]	1	0.27(4)
La(2)	4*a*	0.5893(2)	−0.0184(3)	0.482(3)	1	0.27(4)
La(3)	4*a*	0.5834(2)	0.1778(3)	−0.003(3)	1	0.27(4)
La(4)	4*a*	0.5871(2)	0.6724(3)	0.504(3)	1	0.27(4)
O(1)	4*a*	0.6362(8)	0.6197(8)	0.003(8)	1	0.10(7)
O(2)	4*a*	0.6373(8)	0.1222(8)	0.507(8)	1	0.10(7)
O(3)	4*a*	−0.0473(7)	0.0367(7)	0.002(8)	1	0.01(7)
O(4)	4*a*	−0.0433(7)	0.5431(6)	0.495(9)	1	0.01(7)
Se(1)	4*a*	0.2491(5)	0.5133(1)	0.008(3)	1	0.04(6)
Se(2)	4*a*	0.5746(2)	0.8288(4)	0.004(5)	1	0.29(5)
Se(3)	4*a*	0.5632(2)	0.3264(4)	0.489(5)	1	0.29(5)
Se(4)	4*a*	0.2487(4)	0.2581(1)	−0.008(5)	1	0.16(5)

[a] Space group $Pna2_1$, a = 17.54146(7) Å, b = 16.48188(7) Å, c = 3.99587(1) Å; R_{wp} = 4.387%, R_p = 2.917%, and χ^2 = 4.46. [b] Coordinate fixed as origin not defined along z in space group $Pna2_1$

from 4.47% to 4.39% for one additional parameter) and suggested complete ordering of Mn(2) over these sites. Details of the final structural model are given in Table 4 with bond lengths in Table 5. The structure is illustrated in Figure 9, and refinement profiles are shown in Figure 10. β-$La_2O_2MnSe_2$ orders antiferromagnetically at low temperatures as discussed below and although no additional peaks were observed in the backscattered data, some scattering from the long-range magnetic structure may be present; this has not been modeled and is thought to be the reason for the slightly negative thermal displacement parameters for both Mn sites obtained from these data. The models for β-$La_2O_2MnSe_2$ obtained from refinements using 12 and 295 K data can be used to compare the *Ama*2 and $Pna2_1$ structures. The distortion from *Ama*2 symmetry is very slight, and the main distortion involves ordering of the Mn(2) cations over the sites above and below the MnSe planes. The most significant change in lattice parameters at the phase transition is in

Table 5. Selected Bond Lengths for β-$La_2O_2MnSe_2$ from Combined Refinement Using 12 K XRPD and NPD (Backscattered) Data in Space Group $Pna2_1$

Mn(1)−O(1)	2.13(1) Å	La(2)−O(2)	2.47(1) Å
Mn (1)−O(2)	1.87(1) Å	La(2)−O(4)	2.34(3) Å, 2.36(1) Å, 2.43(3) Å
Mn(1)−Se(1)	2.76(1) Å, 3.00(1) Å	La(2)−Se(2)	3.17(1) Å
Mn(1)−Se(4)	2.86(1) Å, 3.01(1) Å	La(3)−O(2)	2.36(3) Å, 2.43(3) Å
Mn(2)−Se(1)	2.539(6) Å	La(3)−O(4)	2.33(1) Å
Mn(2)−Se(2)	2.615(6) Å	La(3)−Se(3)	3.16(1) Å
Mn(2)−Se(4)	2.53(2) Å, 2.61(2) Å	La(3)−Se(4)	3.085(9) Å
La(1)−O(1)	2.48(1) Å	La(4)−O(1)	2.34(3) Å, 2.35(3) Å
La(1)−O(3)	2.35(3) Å, 2.36(3) Å, 2.44(1) Å	La(4)−O(3)	2.34(1) Å
La(1)−Se(3)	3.19(1) Å	La(4)−Se(4)	3.102(9) Å

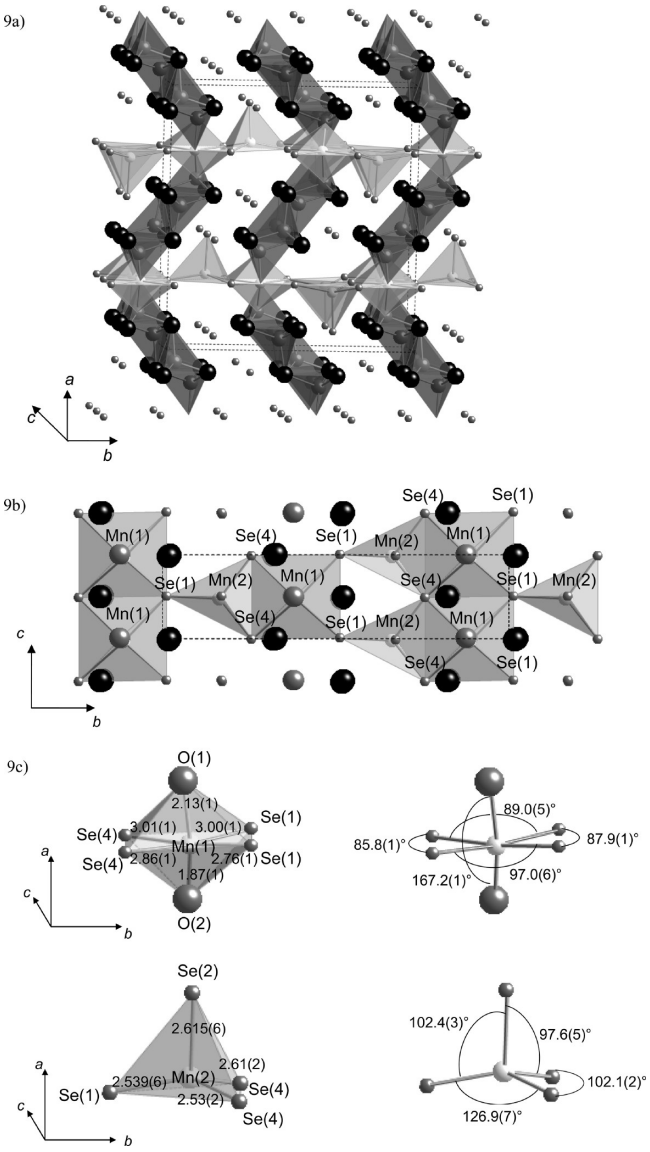

Figure 9. Low temperature structure of β-$La_2O_2MnSe_2$ described by $Pna2_1$ symmetry (a) showing unit cell, (b) viewed down [100] direction showing connectivity of MnSe plane with MnSe polyhedra in light gray and OLa_4 tetrahedra in dark gray with Se and La atoms shown as gray and black spheres, respectively, and (c) showing bond lengths (in Å) and angles of Mn(1) and Mn(2) polyhedra.

the *a* parameter, which is perhaps unsurprising given that the major change involves Mn ordering over sites closely separated along *a* affecting bonding in this direction. This results in a structure with chains of $Mn(2)Se(4)_2Se(2)Se(1)$ tetrahedra corner-linked through Se(4) along the [001] direction with these chains above and below the MnSe planes alternating along [010]. As a result of the Mn(2) ordering, the Se(2) anions move closer to the MnSe sheets. The displacement of the M(2) sites, to give tetrahedral coordination rather than trigonal bipyramial coordination, is unsurprising given the zinc blende structure of the metastable β phase of MnSe with corner-linked $MnSe_4$ tetrahedra[24] and the tetragonal phase of β-FeSe with layers of edge-shared $FeSe_4$ tetrahedra.[25]

Structure of β-$La_2O_2FeSe_2$. XRPD data collected for β-$La_2O_2FeSe_2$ were similar to those obtained at low temperatures for β-$La_2O_2MnSe_2$. However, the weak 410 reflection was observed at room temperature and below for the iron analogue. β-$La_2O_2FeSe_2$ was also found to be weakly SHG active suggesting that low symmetry primitive structure is also acentric, consistent with space group $Pna2_1$. SAED data were collected for β-$La_2O_2FeSe_2$ at room temperature, and diffraction patterns down the [010] and [110] zone axes are shown in Figure 11. These data are consistent with a $Pna2_1$ space group at room temperature, though we could not obtain a diffraction pattern down the [001] zone axis to confirm the presence of $hk0$ $k \neq 2n$ reflections.

The ordered model of $Pna2_1$ symmetry was used in structural refinements for β-$La_2O_2FeSe_2$, and structural details and bond lengths are given in Tables 6, 7, 8, and 9. A small impurity content (~2.6% by weight) was detected and attributed to a ZrCuSiAs-like phase with approximate composition $LaFe_{0.5}OSe$. Atomic displacement parameters for all sites refined to very similar values using the 12 K data and so were constrained to have the same value which gave a negligible change to R_{wp}. Refinements using room temperature data suggest some Fe(2) ordering over the 4*a* sites at room temperature (80(1)% ordering, see Table 5) with the degree of ordering increasing on cooling. The room temperature structure of β-$La_2O_2FeSe_2$ is comparable with the low temperature phase of β-$La_2O_2MnSe_2$, although with a slightly smaller volume, consistent with the smaller ionic radius of Fe^{2+} than of Mn^{2+}. Bond valence sum calculations gave valencies of +2.06, +2.12, and +2.01 for Fe(1), Mn(2), and Fe(3) cations and +3.31, +3.02, +2.81, and +2.60 for La(1), La(2), La(3), and La(4), respectively.[17]

XRPD data were also collected on warming β-$La_2O_2FeSe_2$ from 12 to 493 K and on cooling back to 300 K. Unit cell dimensions obtained from these data are shown

(24) Baroni, A. *Z. Kristallogr. Krist.* **1938**, *99*, 336–339.
(25) Hsu, F.-C.; Luo, J.-Y.; Yeh, K.-W.; Chen, T.-K.; Huang, T.-W.; Wu, P. M.; Lee, Y.-C.; Huang, Y.-L.; Chu, Y. Y.; Yan, D.-C.; Wu, M.-K. *Proc. Natl. Acad. Sci. U.S.A.* **2008**, *105*(38), 14262–14264.

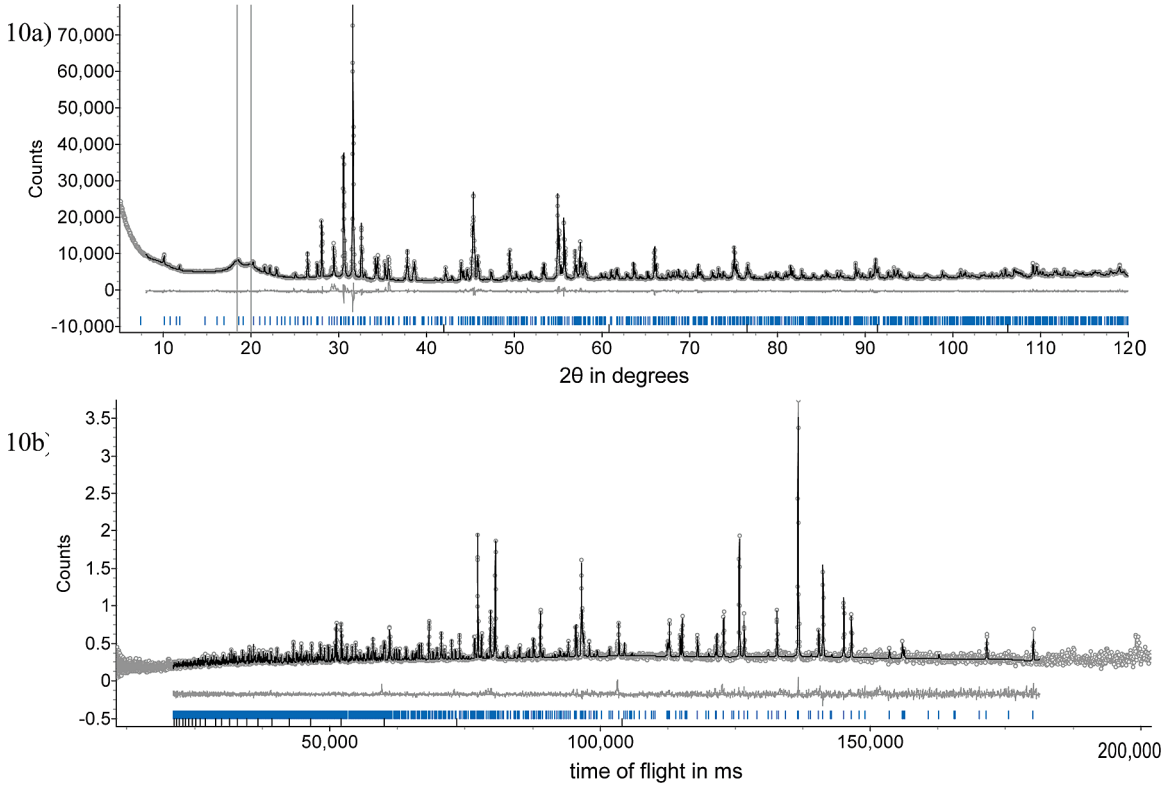

Figure 10. Rietveld refinement profiles from combined refinement using 12 K XRPD (a) and NPD backscattered data (b) for β-$La_2O_2MnSe_2$, refined in space group $Pna2_1$ (observed and calculated patterns shown in gray and black, respectively, with difference profile and peak positions shown below).

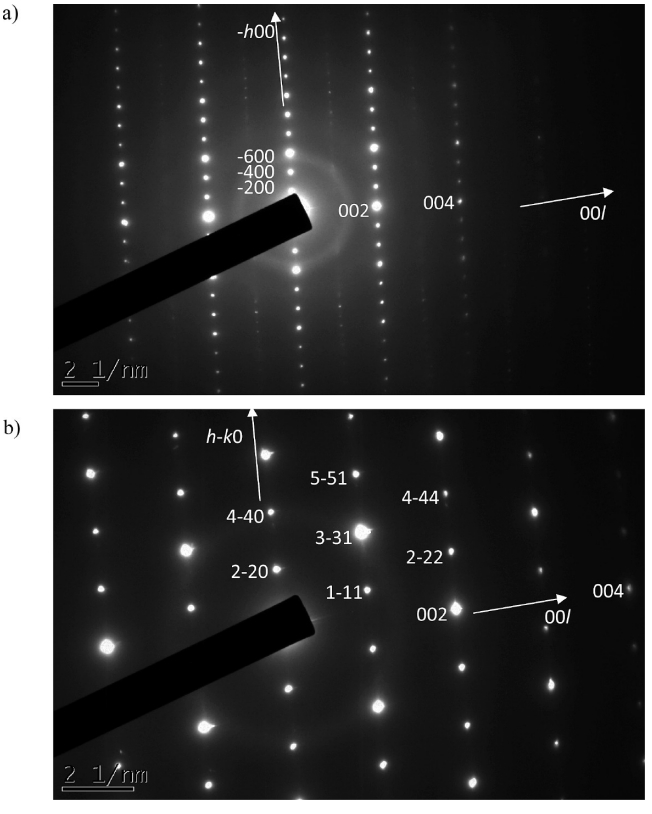

Figure 11. SAED patterns taken down (a) [010] zone axis and (b) [110] zone axis at room temperature for β-$La_2O_2FeSe_2$.

in Figure 5b and clearly show a phase transition at ~373 K. The weak 410 reflection was not visible in data collected

Table 6. Structural Parameters from Combined Refinement for β-$La_2O_2FeSe_2$ Using Room Temperature XRPD and NPD (Backscattered) Data[a]

	Wyckoff site	x	y	z	occupancy	B_{eq}/Å^2
Fe(1)	4*a*	0.2485(5)	0.8837(1)	−0.007(3)	1	1.32(7)
Fe(2)	4*a*	0.7759(5)	0.8367(7)	−0.018(4)	0.80(1)	0.8(1)[c]
Fe(3)	4*a*	0.724(2)	0.837(3)	0.028(8)	0.19(1)	0.8(1)[c]
La(1)	4*a*	0.5925(2)	0.4789(3)	0[b]	1	0.56(9)
La(2)	4*a*	0.5923(2)	−0.0214(3)	0.487(1)	1	0.31(8)
La(3)	4*a*	0.5883(2)	0.1750(3)	−0.051(1)	1	0.01(7)
La(4)	4*a*	0.5836(1)	0.6754(3)	0.488(2)	1	0.11(7)
O(1)	4*a*	0.6430(6)	0.6190(8)	−0.019(6)	1	0.4(1)
O(2)	4*a*	0.6421(5)	0.1210(8)	0.490(5)	1	0.2(1)
O(3)	4*a*	−0.0441(5)	0.0437(6)	−0.007(5)	1	0.1(1)
O(4)	4*a*	−0.0459(6)	0.5359(7)	0.482(6)	1	0.3(1)
Se(1)	4*a*	0.2542(4)	0.5147(1)	−0.034(2)	1	0.50(7)
Se(2)	4*a*	0.5605(2)	0.8279(3)	−0.006(2)	1	0.59(8)
Se(3)	4*a*	0.5755(2)	0.3292(4)	0.495(2)	1	0.48(8)
Se(4)	4*a*	0.2567(3)	0.2494(1)	−0.009(3)	1	0.64(6)

[a] Space group $Pna2_1$, a = 17.34530(5) Å, b = 16.41198(6) Å, c = 3.99684(1) Å; R_{wp} = 2.765%, R_p = 1.878%, and χ^2 = 5.62. [b] Co-ordinate fixed as origin not defined along z in space group $Pna2_1$. [c] Atomic displacement parameters constrained to be equal.

at 493 K. This transition is similar to that observed for β-$La_2O_2MnSe_2$ in that it is a continuous and fully reversible transition; it is most easily observed from changes in the a lattice parameter. The 493 K data could be fitted well with a model of *Ama*2 symmetry, consistent with that described for β-$La_2O_2MnSe_2$.

Physical Properties. The zero-field-cooled (ZFC) and field-cooled (FC) magnetic susceptibility of β-$La_2O_2MnSe_2$ and β-$La_2O_2FeSe_2$ were measured in applied field of 1000 Oe (see Figure 12). Magnetic measurements on

Table 7. Selected Bond Lengths for β-$La_2O_2FeSe_2$ from Combined Refinement Using Room Temperature XRPD and NPD (Backscattered) Data in Space Group $Pna2_1$

Fe(1)−O(1)	1.83(1) Å	La(1)−O(1)	2.46(1) Å
Fe(1)−O(2)	1.90(1) Å	La(1)−O(3)	2.39(2) Å, 2.40(1) Å, 2.44(2) Å
Fe(1)−Se(1)	2.86(1) Å, 3.01(1) Å	La(1)−Se(3)	3.170(9) Å, 3.193(9) Å
Fe(1)−Se(4)	2.97(1) Å, 2.98(1) Å	La(2)−O(2)	2.49(1) Å
Fe(2)−Se(1)	2.47(1) Å	La(2)−O(4)	2.33(2) Å, 2.37(2) Å, 2.41(1) Å
Fe(2)−Se(3)	2.581(9) Å	La(3)−O(2)	2.41(2) Å, 2.52(2) Å
Fe(2)−Se(4)	2.48(1) Å, 2.54(1) Å	La(3)−O(4)	2.40(1) Å
Fe(3)−Se(1)	2.51(5) Å	La(3)−Se(2)	3.158(8) Å
Fe(3)−Se(2)	2.85(4) Å	La(3)−Se(3)	3.12(1) Å
Fe(3)−Se(4)	2.35(4) Å, 2.59(4) Å	La(3)−Se(4)	3.179(6) Å
		La(4)−O(1)	2.41(2) Å, 2.46(2) Å
		La(4)−O(3)	2.27(1) Å
		La(4)−Se(4)	3.032(6) Å

Table 8. Structural Parameters from Combined Refinement for β-$La_2O_2FeSe_2$ Using 12 K XRPD and NPD (Backscattered) Data[a]

	Wyckoff site	x	y	z	occupancy	B_{eq}/Å^2
Fe(1)	4*a*	0.2526(4)	0.8835(1)	0.000(3)	1	0.07(2)[c]
Fe(2)	4*a*	0.7240(1)	0.8378(2)	0.001(3)	1	0.07(2)[c]
La(1)	4*a*	0.5923(2)	0.4769(2)	0[b]	1	0.07(2)[c]
La(2)	4*a*	0.5919(2)	−0.0200(2)	0.476(2)	1	0.07(2)[c]
La(3)	4*a*	0.5841(1)	0.1774(2)	0.002(1)	1	0.07(2)[c]
La(4)	4*a*	0.5886(1)	0.6742(2)	0.525(2)	1	0.07(2)[c]
O(1)	4*a*	0.6435(4)	0.6195(6)	−0.012(6)	1	0.07(2)[c]
O(2)	4*a*	0.6387(4)	0.1229(5)	0.490(6)	1	0.07(2)[c]
O(3)	4*a*	−0.0483(5)	0.0387(6)	−0.001(6)	1	0.07(2)[c]
O(4)	4*a*	−0.0434(5)	0.5411(6)	0.503(5)	1	0.07(2)[c]
Se(1)	4*a*	0.2487(4)	0.5150(1)	−0.027(2)	1	0.07(2)[c]
Se(2)	4*a*	0.5752(1)	0.8305(3)	−0.011(2)	1	0.07(2)[c]
Se(3)	4*a*	0.5604(2)	0.3264(3)	0.485(2)	1	0.07(2)[c]
Se(4)	4*a*	0.2492(3)	0.2514(1)	−0.003(3)	1	0.07(2)[c]

[a] Space group $Pna2_1$, a = 17.32278(7) Å, b = 16.36224(7) Å, c = 3.98699(1) Å; R_{wp} = 3.470%, R_p = 2.456%, and χ^2 = 4.33. [b] Coordinate fixed as origin not defined along z in space group $Pna2_1$. [c] Atomic displacement parameters constrained to be equal.

β-$La_2O_2MnSe_2$ suggest that it orders antiferromagnetically at low temperatures with a Néel temperature of ~27 K. A plot of inverse susceptibility versus temperature is included in Figure 12, and a Curie−Weiss fit for 200 K ≤ T ≤ 300 K indicates a paramagnetic moment of 5.86 μ_B per formula unit and a Weiss constant of −122 K, consistent with the expected spin-only value of 5.92 μ_B for a Mn^{2+} ion. An additional broad reflection was observed in the 12 K NPD data at ~7.3 Å and a slight shoulder to a peak at ~4.7 Å in the 30° bank. From the short NPD scans collected on warming, additional intensity was observed at ~7.3 Å at 18 and 24 K but not above, consistent with antiferromagnetic ordering below T_N. This broad magnetic reflection is insufficient for us to be able to propose a magnetic structure for the material. Magnetization data for β-$La_2O_2FeSe_2$ show non-Curie−Weiss behavior in the temperature range studied. The susceptibility observed for β-$La_2O_2FeSe_2$ is slightly higher than that observed for the

Table 9. Selected Bond Lengths for β-$La_2O_2FeSe_2$ from Combined Refinement Using 12 K XRPD and NPD (Backscattered) Data in Space Group $Pna2_1$

Fe(1)−O(1)	1.886(9) Å	La(2)−Se(2)	3.14(1) Å, 3.21(1) Å
Fe(1)−O(2)	1.90(1) Å	La(3)−O(2)	2.34(2) Å, 2.44(2) Å
Fe(1)−Se(1)	2.86(1) Å, 3.01(1) Å	La(3)−O(4)	2.34(1) Å
Fe(1)−Se(4)	2.94(1) Å, 2.95(1) Å	La(3)−Se(3)	3.134(9) Å, 3.21(1) Å
Fe(2)−Se(1)	2.449(4) Å	La(3)−Se(4)	3.089(6) Å
Fe(2)−Se(2)	2.580(4) Å	La(4)−O(1)	2.26(2) Å, 2.51(2) Å
Fe(2)−Se(4)	2.50(1) Å, 2.53(1) Å	La(4)−O(3)	2.33(1) Å
La(1)−O(1)	2.50(1) Å	La(4)−Se(2)	3.17(1) Å
La(1)−O(3)	2.36(2) Å, 2.37(2) Å, 2.449(9) Å	La(4)−Se(3)	3.167(9) Å
La(2)−O(2)	2.47(1) Å	La(4)−Se(4)	3.065(7) Å
La(2)−O(4)	2.29(2) Å, 2.373(9) Å, 2.48(2) Å		

metallic iron oxypnictides and doped oxypnictides.[1,26] The (broad) maximum in susceptibility at ~92 K suggests that the material undergoes a transition to an antiferromagnetically ordered state below this temperature. This is consistent with low temperature NPD data in which a small number of additional reflections were observed on cooling below ~95 K. These additional reflections are relatively weak and are only observed in the 30° data bank (see Figure 13), at similar d-spacings to those observed for β-$La_2O_2MnSe_2$ at 12 K. They could not be indexed using a simple commensurate supercell, and the quality of the present data is not sufficient to attempt magnetic structure determination but may suggest that both materials adopt similar magnetic structures at low temperature. The sum of the intensities of magnetic reflections is shown in Figure 14; although the reflections are of low intensity and the data are quite noisy, a $(1 - T/T_N)^\beta$ function with T_N = 91(1) K and β = 0.56(6) fits the intensities reasonably well and gives a Néel temperature consistent with susceptibility data.

The resistance of a sample of β-$La_2O_2MnSe_2$ at room temperature was too high to measure (in excess of 6 GOhms). Diffuse reflectance measurements for β-$La_2O_2MnSe_2$ diluted in NaCl show a decrease in reflectance from 775 nm. The diffuse reflectance spectrum for β-$La_2O_2MnSe_2$ after the Kubelka−Munk treatment is shown in Figure 15. The intercept of the linear increase in the Kubelka−Munk remission function $F = (1 - R)^2/2R$ (where R is the diffuse reflectance) with the energy axis can be used to determine the optical band gap.[10,27] These data suggest an optical band gap of 1.6(1) eV for β-$La_2O_2MnSe_2$, with some higher energy interband transitions also observed. The optical band gap of $CeMn_{0.5}OSe$ is reported as 2.01 eV.[5]

The resistivity of β-$La_2O_2FeSe_2$ was measured on cooling and on warming between 300 and 150 K (for T < 150 K, the resistance of the sample was too high to measure), and the results are shown in Figure 16a. The room temperature resistivity is ~10^2 Ω cm. An Arrhenius plot of log(conductivity) versus reciprocal temperature gave a straight line (see Figure 16b), and the activation energy was calculated as 0.35 eV, indicating an electronic band

(26) Cimberle, M. R.; Canepa, F.; Ferretti, M.; Martinelli, A.; Palenzona, A.; Siri, A. S.; Tarantini, C.; Tropeano, M.; Ferdeghini, C. *J. Magn. Magn. Mater.* **2009**, *321*, 3024–3030.

(27) Tandon, S. P.; Gutpa, J. P. *Phys. Status Solidi* **1970**, *38*, 363–366.

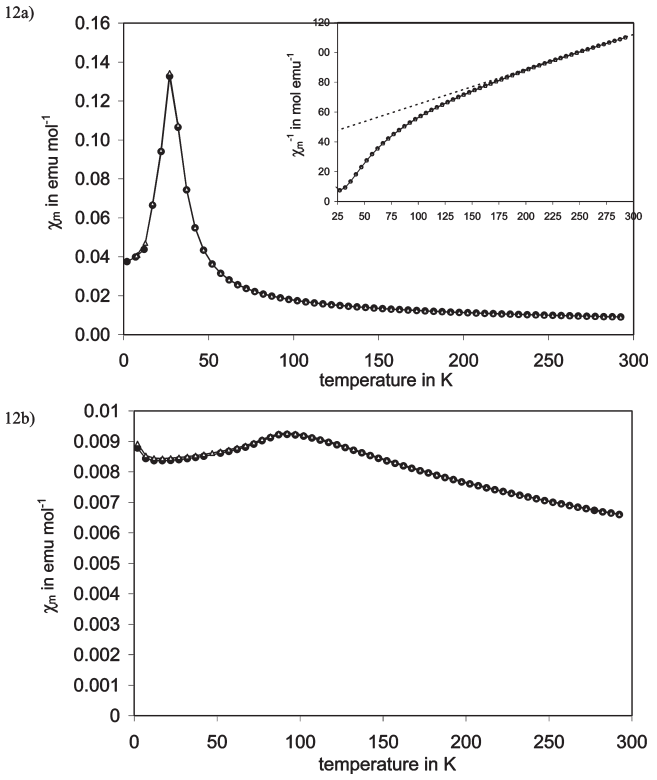

Figure 12. Susceptibility measurements for (a) β-$La_2O_2MnSe_2$ and (b) β-$La_2O_2FeSe_2$ with field-cooled and zero-field-cooled data shown with filled circles and open triangles, respectively, with plot of inverse susceptibility versus temperature for β-$La_2O_2MnSe_2$ shown inset to Figure 6a. Measurements were carried out in an applied field of 1×10^3 Oe.

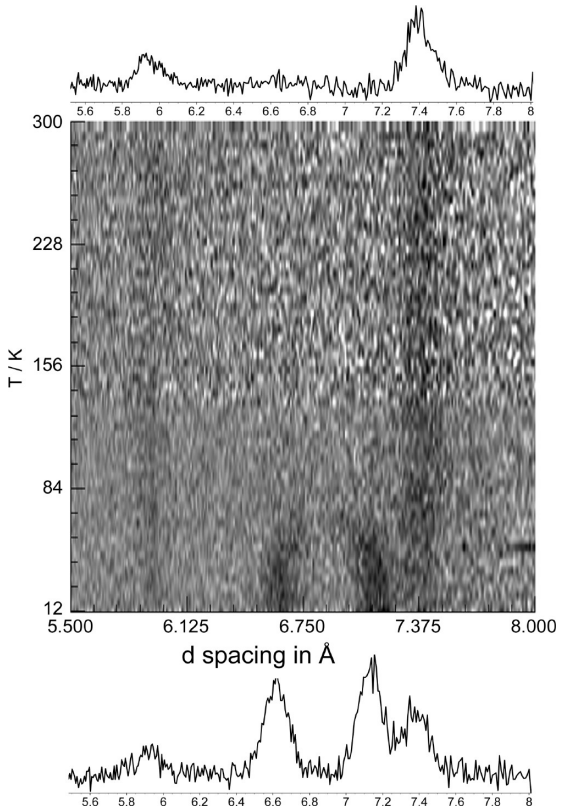

Figure 13. 2D plot and data sets for β-$La_2O_2FeSe_2$ showing additional reflections at low temperatures in the 30° data bank.

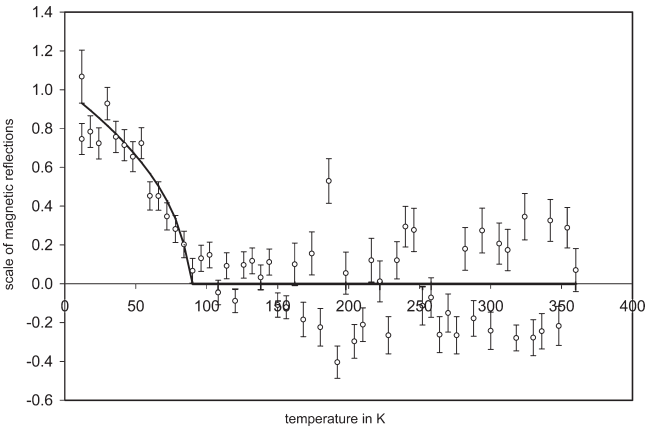

Figure 14. Plot showing the change in intensity of magnetic reflections for β-$La_2O_2FeSe_2$ as a function of temperature where the intensity has been modeled relative to the intensity at 12 K. Open circles show the calculated data, and the solid line has been calculated using the function described in the text.

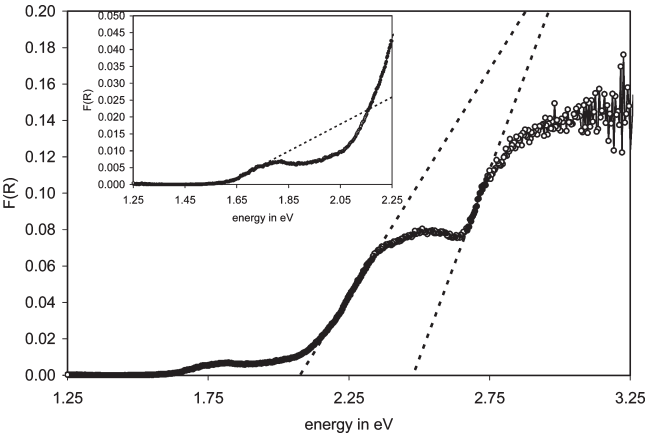

Figure 15. Diffuse reflectance spectrum for β-$La_2O_2MnSe_2$ diluted in dry NaCl after Kubelka−Munk treatment showing two interband transitions and the band gap in the visible region; inset, lowest energy region.

gap of ~0.7 eV. These results show that β-$La_2O_2FeSe_2$ is a semiconductor in the temperature range studied. The room temperature resistivity of β-$La_2O_2FeSe_2$ is several orders of magnitude greater than that of LaFeOAs ($\sim 5 \times 10^{-3}$ Ω cm),[1] and metallic α-FeSe ($\sim 1 \times 10^{-3}$ Ω cm)[28] and is more comparable to that of $La_2O_2Fe_2OSe_2$ ($\sim 10^2$ Ω cm)[29] which contains Fe_2OSe_2 layers with Fe^{2+} cations linked by in-plane oxide anions and out-of-plane selenide anions. The band structures of LaFeOAs and FeSe systems are similar with the electronic structure near the Fermi level (E_F) dominated by Fe−Fe interactions, with As/Se p states significantly below E_F and having only moderate hybridization with Fe. Both are low carrier density metals.[30] The $La_2O_2Fe_2OQ_2$ (Q = S, Se) systems are found to have significant band narrowing relative to

(28) Mizuguchi, Y.; Tomioka, F.; Tsuda, S.; Yamaguchi, T.; Takano, Y. *Appl. Phys. Lett.* **2008**, *93*, 152505.
(29) Zhu, J.-X.; Yu, R.; Wang, H.; Zhao, L. L.; Jones, M. D.; Dai, J.; Abrahams, E.; Morosan, E.; Fang, M.; Si, Q. *Phys. Rev. Lett.* **2009**, *104*, 216405.
(30) (a) Singh, D. J.; Du, M.-H. *Phys. Rev. Lett.* **2008**, *100*, 237003. (b) Subedi, A.; Zhang, L.; Singh, D. J.; Du, M. H. *Phys. Rev. B* **2008**, *78*, 134514.

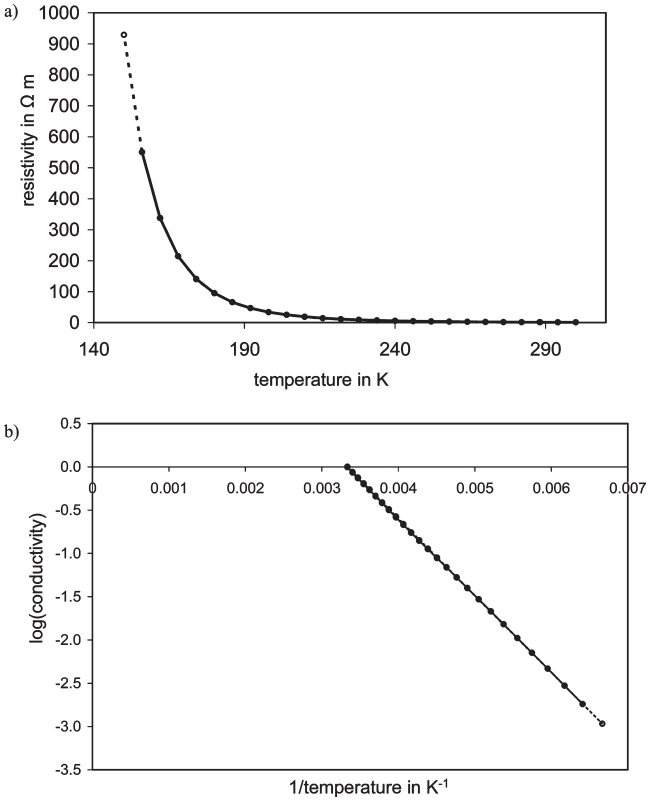

Figure 16. (a) Resistivity of β-$La_2O_2FeSe_2$ and (b) log(conductivity) vs reciprocal temperature, with data collected on cooling shown by the dashed line and open circles and data collected on warming shown by closed circles and the solid line.

these systems and are Mott insulators.[29] β-$La_2O_2FeSe_2$ is presumably also on the insulating side of a Mott boundary.

Conclusions

In conclusion, we describe here the synthesis and structural and physical characterization of two new oxyselenide materials β-$La_2O_2MSe_2$ (M = Mn, Fe). They adopt a new structure type which has been determined from powder X-ray and neutron diffraction data. The structure is orthorhombic, *Ama*2 with a = 17.5 Å, b = 16.6 Å, and c = 4.0 Å made up of alternating layers of edge- and corner-linked MSe_n polyhedra. On cooling, an order−disorder structural phase transition is observed and the symmetry is lowered to $Pna2_1$. Both manganese and iron analogues are antiferromagnetic at low temperature. β-$La_2O_2MnSe_2$ is an insulator at room temperature with an optical band gap of 1.6 eV while β-$La_2O_2FeSe_2$ is a semiconductor in the temperature range of 150−300 K with a band gap of ~0.7 eV.

Acknowledgment. We are grateful to EPSRC for funding (Grant EP/F066422/1) and ISIS for the provision of NPD time. We thank Dr. R. Smith for collection of NPD data through the GEMXpress scheme and Dr. A. Daoud-Aladine for assistance with NPD data collection on HRPD. We are very grateful to Dr. S. Halasyamani for SHG measurements and to Dr. Y. Takayashi for SQUID measurements. We are grateful to Dr. A. Beeby for diffuse reflectance measurements.

Supporting Information Available: Crystallographic information files: $La_2O_2MnSe_2$ at room temperature; $La_2O_2MnSe_2$ at 12 K; $La_2O_2FeSe_2$ at room temperature; $La_2O_2FeSe_2$ at 12 K (CIF). This material is available free of charge via the Internet at http://pubs.acs.org.